SUPPORTING INFORMATION

Microswimmers with Heat Delivery Capacity for 3D Cell Spheroid Penetration

Miguel A. Ramos-Docampo,[†,§] *Marina Fernández-Medina,*[†] *Essi Taipaleenmäki,*[†] *Ondrej Hovorka,*[¤] *Verónica Salgueiriño*[§]* *and Brigitte Städler*[†]*

†Interdisciplinary Nanoscience Center (iNANO), Aarhus University, Gustav Wieds Vej 14, 8000 Aarhus (Denmark)

§Departamento de Física Aplicada, Universidade de Vigo, 36310 Vigo (Spain)

[¤]Faculty of Engineering and Physical Sciences, University of Southampton, SO16 7QF, Southampton (UK)

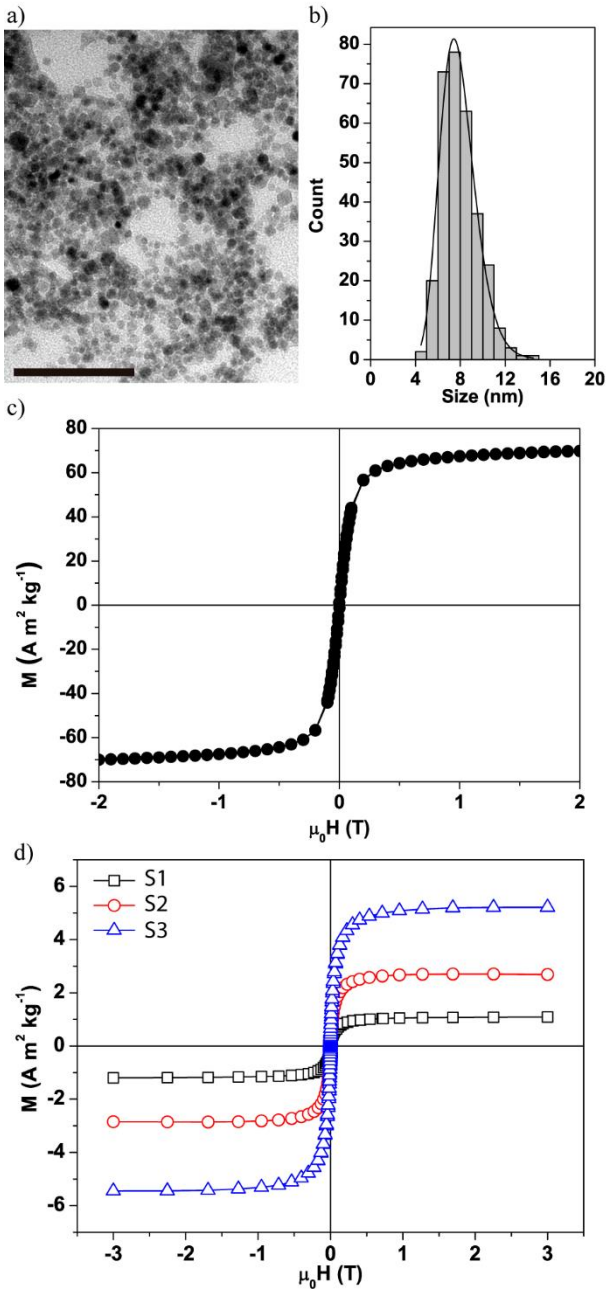

Figure S1. Characterization of MF-NPs. a) Representative TEM image (scale bar: 200 nm) and b) size distribution (log-normal fit) of the MF-NPs. c) M-H curve of the MF-NPs at room temperature. d) M-H curves of swimmers S1-S3 at room temperature.

Assessment of the magnetic content in swimmers S1, S2 and S3:

In order to characterize the three samples in more detail, magnetic measurements (magnetization *versus* field (M *vs*. H) curves) were obtained (Figure S1d). These results allowed us to confirm that S1 contained the lowest amount of magnetic material and S3 contained the highest amount of magnetic material, as reflected by the values of saturation

magnetization (1.15, 2.77 and 5.34 Am^2kg^{-1} (T = 300 K), for samples S1, S2 and S3, respectively). Taking these values of saturation magnetization into account and using the value of saturation magnetization of the sample of manganese ferrite nanoparticles as reference (M_S = 69.80 Am^2kg^{-1} (T = 300 K), please see Figure S1c in the Supplementary Information), we estimated the weight percentage of magnetic nanoparticles present in the three samples to be 1.6% in S1, 4.0% in S2, and 7.6% in S3.

In other words, swimmers belonging to S1 have 1.6 wt. % of magnetic nanoparticles, swimmers belonging to S2 have 4.0 wt. % of magnetic nanoparticles, and swimmers belonging to S3 have 7.6 wt. % of magnetic nanoparticles.

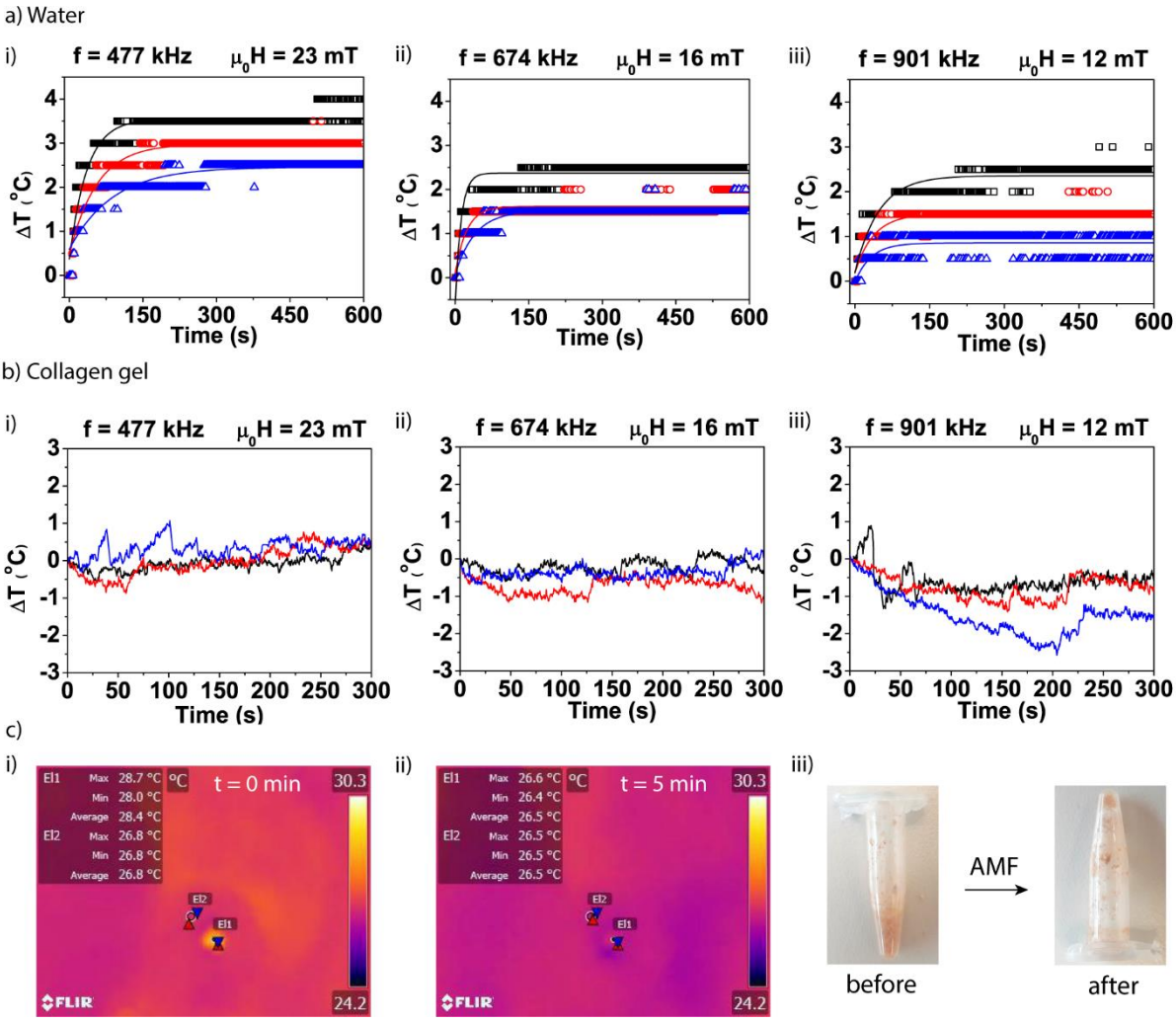

Figure S2. Magneto-caloric measurements of swimmers S1 (black), S2 (red) and S3 (blue) in a) water and b) collagen gel at different working conditions of the AMF. c) IR photographs (i/ii) and standard photographs (iii) of the phase change in collagen gel after applying the AMF to S1 at f = 477 kHz over 5 min.

Evaluation of Heating Performance

The common method to evaluate the heating performance of magnetic nanoparticles employs a calorimetric technique, in order to obtain the SAR (specific absorption rate) parameter. This parameter permits the evaluation of the suitability or efficiency of magnetic nanoparticles for heat delivery.

The SAR value of a given system can be calculated as follows:

$$SAR = \frac{C_p}{m_{MNP}} \left|\frac{dT}{dt}\right|_{t=0} \quad \text{(Eq. S1)}$$

where C_p is the heat capacity of the sample, m_{MNP} the mass of the magnetic material, and $\left|\frac{\mathrm{dT}}{\mathrm{dt}}\right|_{\mathrm{t=0}}$ is the heating rate.

The heating rate can be calculated considering the temperature evolution profile in non-adiabatic conditions:

$$T(t) = \lambda_Q \left|\frac{dT}{dt}\right|_{t=0} \left(1 - \exp\left(-\frac{t}{\lambda_Q}\right)\right) \quad \text{(Eq. S2)}$$

where λ_Q is a relaxation constant, which depends on the heat capacity, the surface of the sample, and the heat transfer coefficient between the sample and the medium.

Eq. S2 allows for calculating the heating rate by fitting the initial slope of the curve to

$$|dT/dt|_{t=0} = \Delta T/\lambda_Q \quad \text{(Eq. S3)}$$

where ΔT is the temperature increment after switching on the AMF, necessary to calculate the SAR value.

Additionally, the heating rate and the dM/dH ratio can be related throughout the following expression, which also conveys the final temperature difference

$$\left(\frac{\omega H_0^2}{2\rho}\right)\bar{\chi} = SAR = \frac{C_p}{m_{MNP}} \left|\frac{dT}{dt}\right|_{t=0} \quad \text{(Eq. S4)}$$

where ω is the angular frequency, H_0 is the amplitude of the alternating magnetic field employed, ρ the density of the medium, and $\bar{\chi}$ the dynamic susceptibility of the material, which depends on the static susceptibility (dM/dH). Since M is usually expressed in Am^2/kg, it also relates to the loading content.

Whereas the static magnetic susceptibility is an intrinsic property of the material and specifies the degree of magnetization of a material with respect to an applied magnetic field, and can be calculated as follows:

$$\chi_0 = \left(\frac{dM}{dH}\right) \qquad \text{(Eq. S5)}$$

the AC or dynamic magnetic susceptibility accounts for the calculation of the SAR value in the case of magnetic hyperthermia, and can be readily estimated through the following expression:

$$\bar{\chi} = \frac{\chi_0}{1+i\omega\tau} \qquad \text{(Eq. S6)}$$

being $\omega = 2\pi f$, and from which the real (χ') and imaginary (χ'') components of the susceptibility are:

$$\chi' = \frac{\chi_0}{1+(\omega\tau)^2} \qquad \text{(Eq. S7a)}$$

$$\chi'' = \frac{\chi_0\omega\tau}{1+(\omega\tau)^2} \qquad \text{(Eq. S7b)}$$

According to these expressions, besides the type of material, the susceptibility depends on the frequency at which the magnetic field is oscillating (ω) and the relaxation time (τ) of the magnetic moment of the nanoparticle.

Additionally, the power dissipation can be expressed as:

$$P = \pi\mu_0\chi_0 H_0^2 f \frac{2\pi f\tau}{1+(2\pi f\tau)^2} \qquad \text{(Eq. S8)}$$

indicating that the heat capability of the magnetic nanoparticles is not frequency field and magnitude (H_0) dependent.

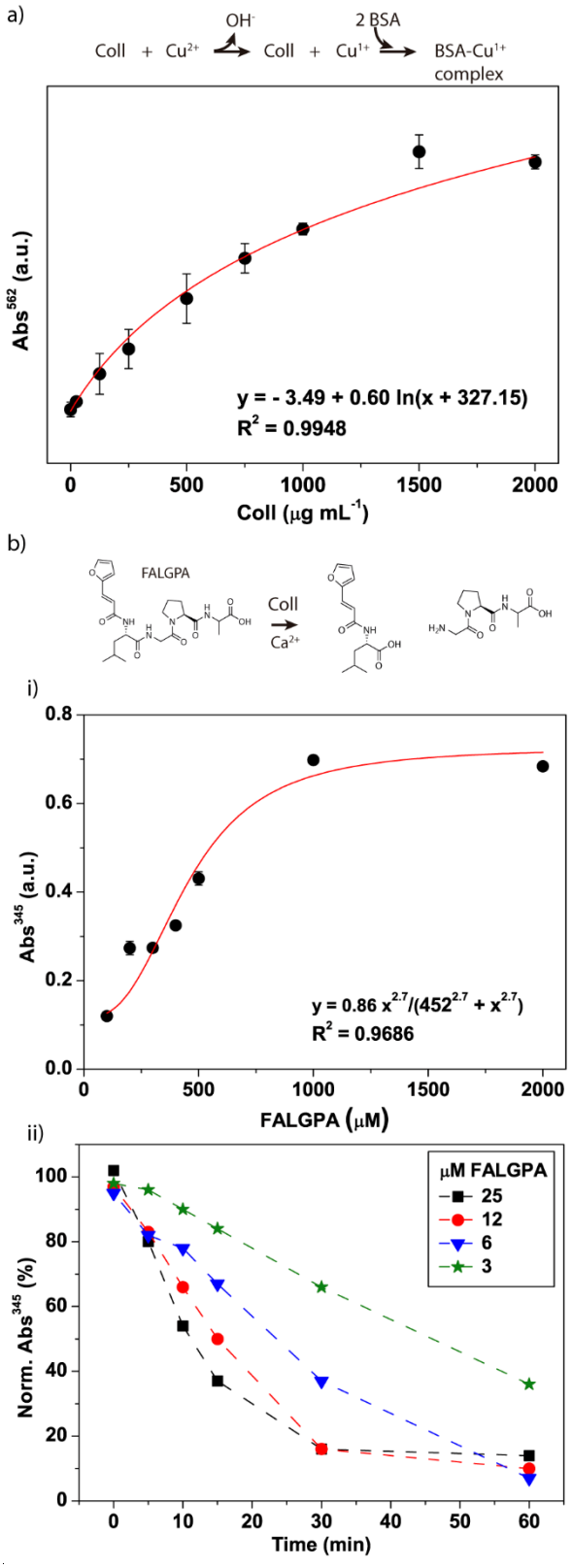

Figure S3. S1-C characterization. a) BCA mass assay of free Coll used for the further assessment of the Coll mass per swimmer. b) i) Activity assay of free Coll, and ii) catalytic performance of free Coll for different FALGPA concentrations. Based on the results from the

BCA assay, the Coll concentration was adjusted to 225 μg mL^{-1}, which corresponded to the amount of enzyme deposited on S1-C, and FALGPA (concentrations ranging from 3 to 25 μM) was systematically added. The substrate conversion was assessed over 60 min, measuring the absorbance at λ = 345 nm at different time points. More concentrated solutions contributed to a faster FALGPA conversion, in agreement to enzyme kinetics k ~ [S], that is, the rate constant is proportional to the concentration of substrate. The calcium concentration was 0.36 mM for all experiments, according to standard protocols.

First, standard solutions of free Coll ranging from 25 to 2000 μg mL^{-1} were prepared and used to obtain a calibration curve using the BCA assay by measuring the absorbance at λ = 542 nm. The data from the BCA assay exhibited a logarithm trend that reached a plateau for Coll concentrations higher than 1500 μg mL^{-1} (Figure S3a).

Next, S1-C were analyzed using the same assay, and the absorbance value obtained was interpolated in the calibration curve. The Coll concentration was found to be 225 (± 8) μg mL^{-1}, which corresponded to ~4×10^{-9} μg enzyme per S1-C.

The enzyme kinetics obeyed a non-Michaelis-Menten profile, *i.e.*, a sigmoidal increase of the reaction rate along with substrate concentration (FALGPA) was found (Figure S3bi). This behavior was expected, since Coll needs either Ca^{2+} or Zn^{2+} ions to be activated. The enzyme was saturated when the substrate reached a concentration of ~1000 μM. The maximum velocity achieved by the enzyme was 0.86 μmol s^{-1}, and the microscopic dissociation constant resulted to be 452 μM, similar to others already reported.[1] The exponent of the fitting (> 0) indicated a positive cooperative binding, and also agreed to the active binding sites of collagenase, as it uses two calcium ions to be activated.[2] The enzyme kinetics increased with increasing substrate concentration (Figure S3bii). The Coll activity upon deposition on S1 was calculated by means of the following equations:

$$Units/_{mL\ Coll} = \frac{\Delta Abs^{345} \times V_f \times DL}{\varepsilon_{FALGPA} \times V_{Coll}}$$

$$Units/_{mg\ solid} = \frac{Units/mL\ Coll}{mg\ solid/mL\ Coll}$$

where ΔAbs^{345} stands for the absorbance at λ = 345 nm, V_f for the volume of the sample, DL for the dilution factor, ε_{FALGPA} for the extinction coefficient for FALGPA, and V_{Coll} for the volume of added Coll.

The value obtained for the activity of the free Coll when using FALGPA as substrate was 11.18 U mg^{-1} (which was considered to be 100% activity). The activity value after the enzyme was immobilized was 3.35 U mg^{-1} (which translated into 30% of the initial activity).

The enzyme capacity, that is, the mol-to-mass ratio between enzyme and substrate, was ~0.45 nmol mg^{-1} for the highest FALGPA concentrations (1 mM), in order to be comparable to collagen in the subsequent experiments. This relation states that when all the active sites in the enzyme are occupied (enzyme capacity = 0), the enzyme is at its maximum capacity and increasing the substrate concentration will not increase the reaction rate.

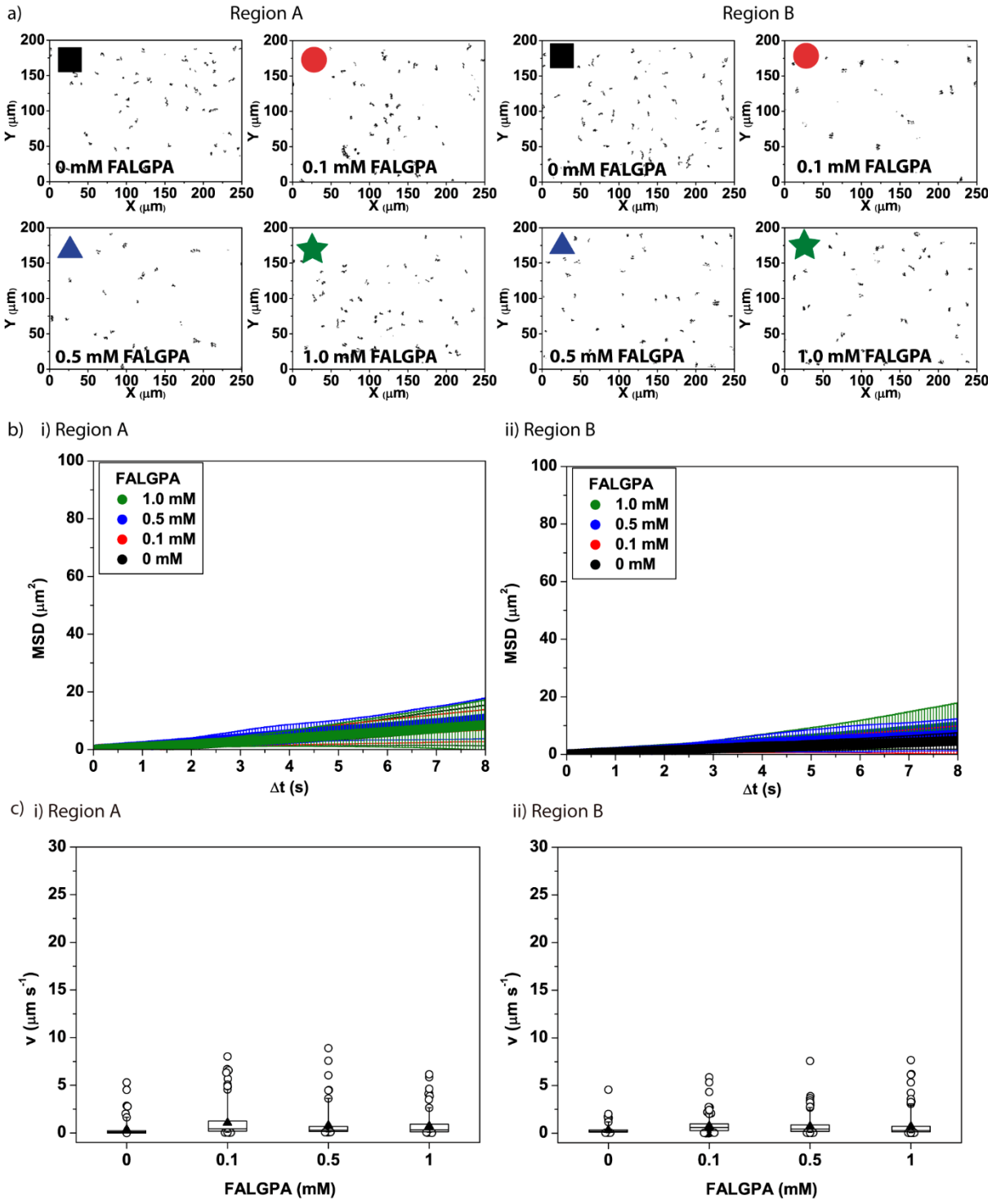

Figure S4. S1-C in buffer solution, 0.36 mM calcium. a) Extracted trajectories and b) MSD plots of S1-C swimmers mixed with 0 mM (black square), 0.1 mM (red circle), 0.5 mM (blue triangle), and 1 mM (green star) FALGPA for Regions A and B using 0.36 mM calcium to initiate the calcium gradient. c) Whisker plots of the velocity for S1-C undergoing Brownian motion in Regions A (i) and B (ii).

Dunderdale *et al.* reported the characteristics of particle motion to differentiate between (enhanced) Brownian motion, nanopropulsion and directed motion, according to the expression $MSD(\Delta t) = 4D\Delta t + \frac{v^2\tau_r^2}{2}\left[\frac{2\Delta t}{\tau_r} + \exp\left(-\frac{2\Delta t}{\tau_r}\right) - 1\right]$.[3] Thus, particles undergoing Brownian motion present a linear MSD plot, where the slope is directly proportional to the diffusion coefficient (*D*). In a scenario where particles move by nanopropulsion, the MSD plot reveals a linear trend at longer times, being parabolic at shorter Δt ($\ll \tau_r$). For swimmers undergoing directed mobility, the MSD fits to a parabolic curve for all Δt. The diffusion coefficients were extracted from the MSD plots, with values below 0.26 $\mu m^2\ s^{-1}$ in all cases. These low values in diffusivity cannot be considered as enhanced (active) diffusion, but normal (random) Brownian motion. Other studies have been performed using glucose oxidase, urease or catalase as motors, showing diffusion coefficient values that ranged from 1.00 to 1.30 $\mu m^2\ s^{-1}$, when exposed to the optimal substrate concentration.[4]

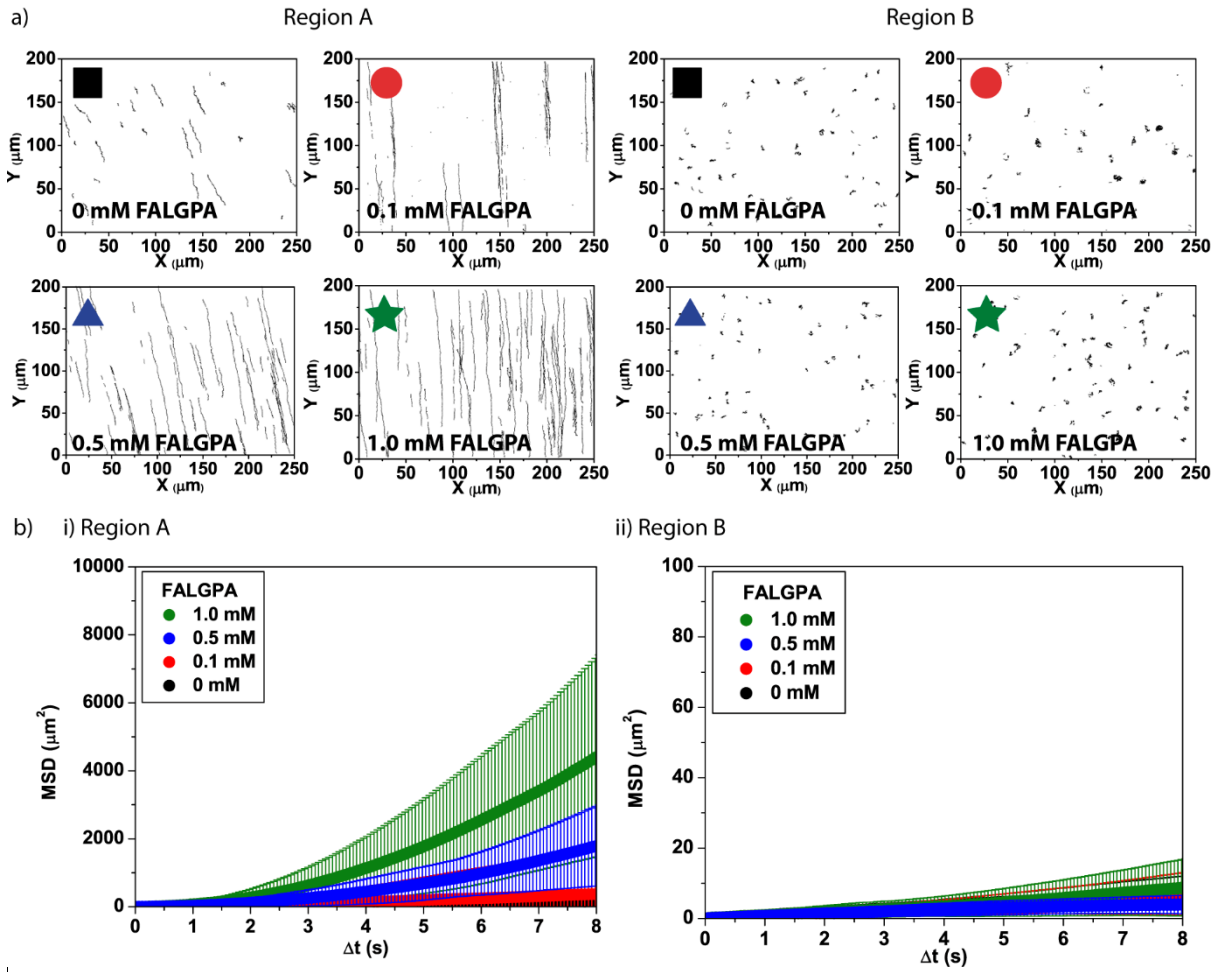

Figure S5. S1-C in buffer solution, 1 mM calcium. a) Extracted trajectories and b) MSD plots of S1-C swimmers mixed with 0 mM (black square), 0.1 mM (red circle), 0.5 mM (blue triangle), and 1 mM (green star) FALGPA for Regions A and B using 1 mM calcium to initiate the calcium gradient.

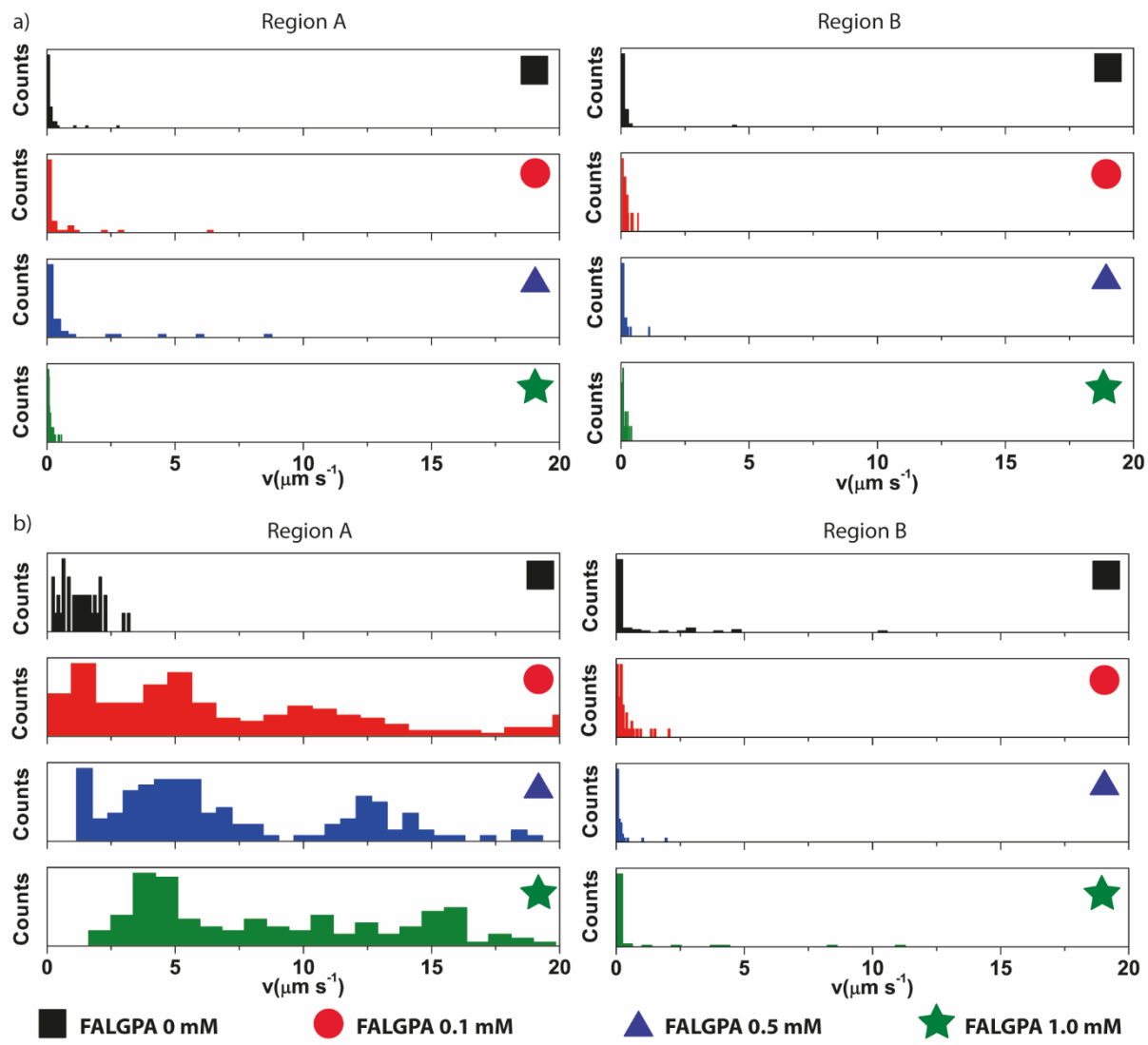

Figure S6. Histograms of S1-C velocities using 0 mM (black square), 0.1 mM (red circle), 0.5 mM (blue triangle), and 1 mM (green star) FALGPA for regions A and B employing 0.36 mM calcium (a) and 1.0 mM calcium (b).

Note that the velocity of swimmers experiencing Brownian motion was determined as the ratio between the radius of gyration and the travelling time as explained in detail in the methods section in the main part of the text.

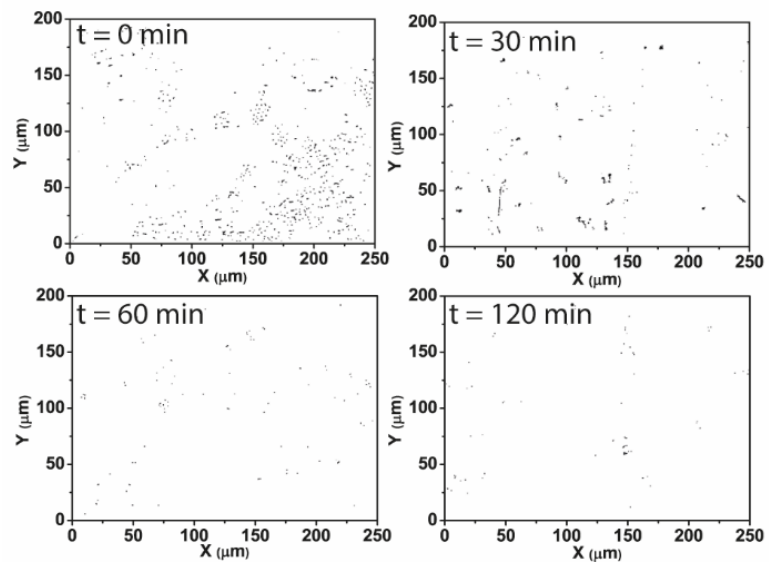

Figure S7. Trajectories of S1-C in collagen gel (cross-linked using 50 % PBS) extracted from movies recorded directly after 1.0 mM calcium addition as well as 30, 60 and 120 min later. No S1-C mobility was observed within the 2 h.

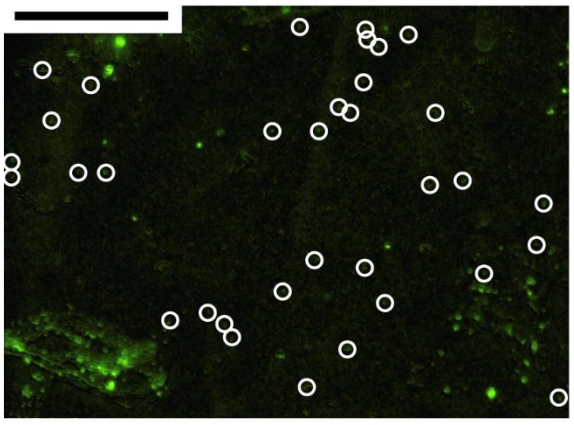

Figure S8. Fluorescent microscopy image of fluorescently-labeled tracer particles at the same position as the movie in Movie S7. Circles indicate weakly fluorescently-labeled tracer particles. These tracer particles do not exhibit locomotion in Movie S7, confirming that only S1-C are mobile. Scale bar: 50 μm.

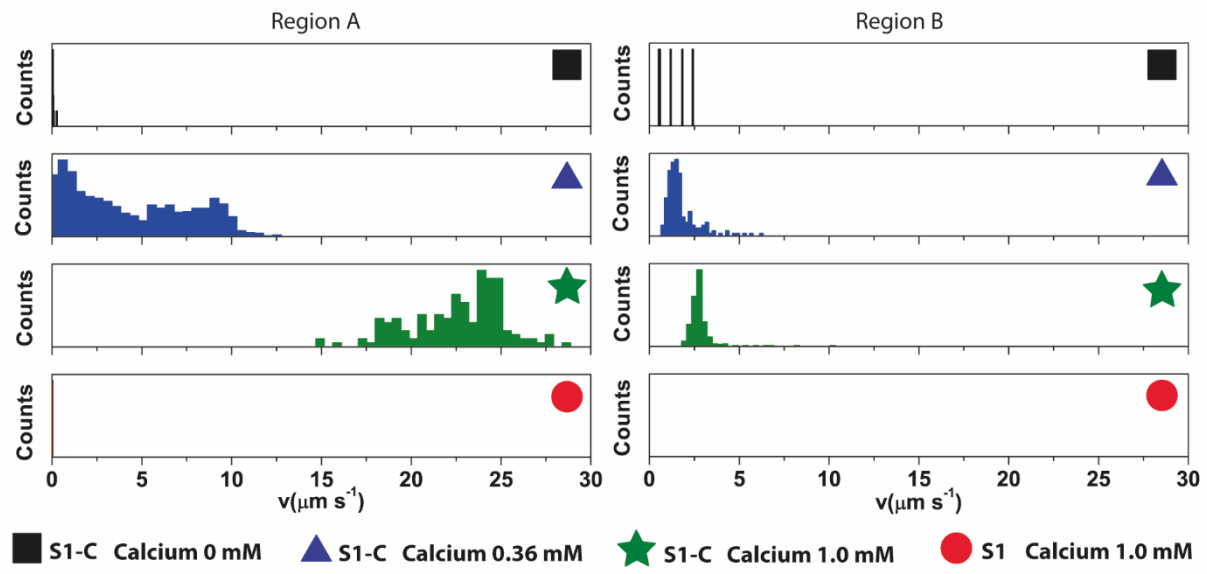

Figure S9. Histograms of S1-C velocities using 0 mM calcium (black square), 0.36 mM calcium (blue triangle) and 1 mM calcium (green star) in regions A and B in a collagen gel. S1 in the presence of 1 mM calcium (red circle) are used as control.

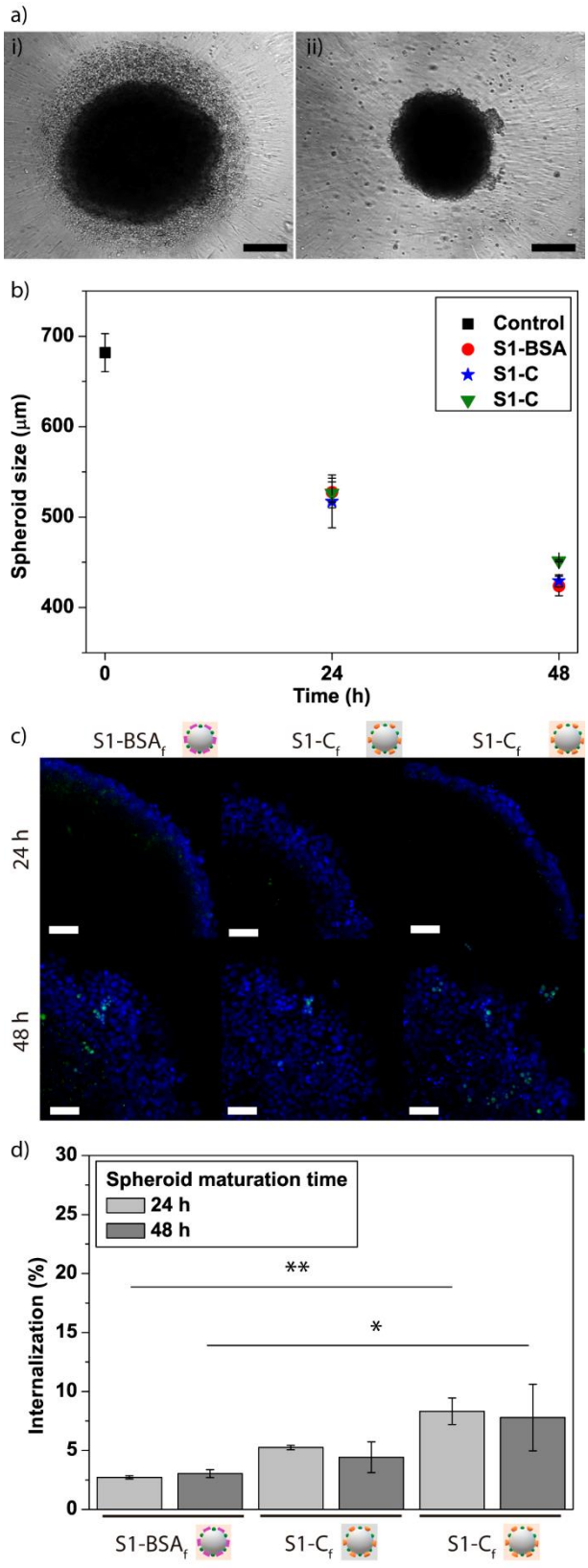

Figure S10. Penetration of S1-C into spheroids. a) Representative bright field microscopy images of the pristine spheroids 24 h (i) and 48 h (ii) after seeding (no incubation with S1-C). The reduction in size is due to condensation of the superstructure. Scale bars: 200 µm. b)

Spheroid size and c) CLSM images of the spheroids aged over 24 h and 48 h, followed by the addition of S1-BSA_f, S1-C_f (no calcium), and S1-C_f for 3 h. Blue channel represents the cell nuclei and green channel represents the labeled swimmers. d) Swimmers located inside of the spheroid (represented as internalization %), determined as the percentage of green pixels in the spheroid area of images. Data represent mean ± SD, n = 2-3, **p < 0.01, *p < 0.05. Scale bars: 50 µm.

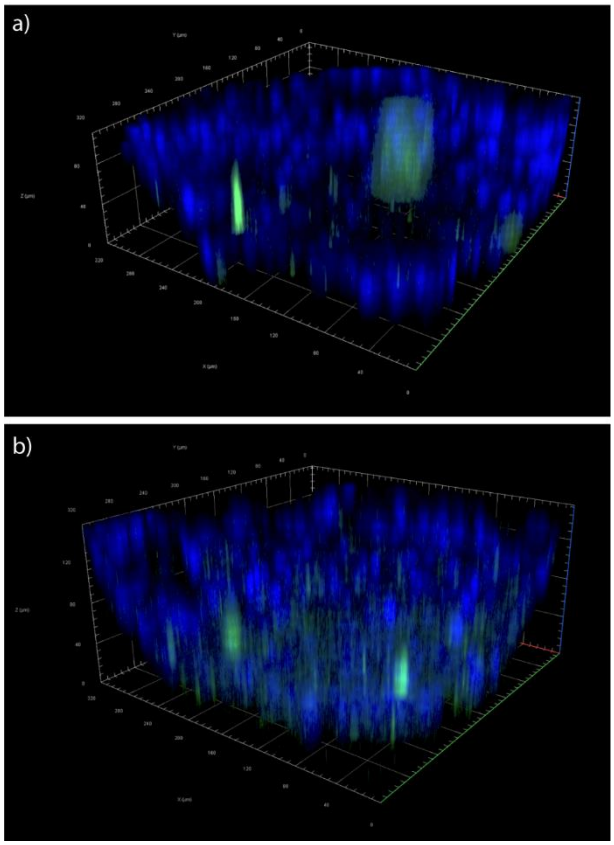

Figure S11. Spheroids 3D reconstruction. CLSM images of the spheroids aged for 48 h, followed by the addition of S1-C_f (no calcium, a) and S1-C_f (b) for 24 h. Blue channel represents the cell nuclei and green channel represents the fluorescently labeled S1-C_f.

Assessing the heating effect of swimmers from magnetic measurements

Magneto-caloric measurements shown in the supporting Fig. S2 suggest that swimmers S1 deliver the best heating rate. In this section we argue that these measurements are fully consistent with the magnetometry data discussed in the main part of the text (Fig. 2(b)).

The main difficulty with interpreting the magnetometry data is in determining the magnetic mass (or magnetic volume) of magnetic nanoparticles, i.e. excluding all non-magnetic contributions relevant under the given experimental settings. This is essential for determining the saturation magnetisation and evaluating the slope of the magnetic moment versus field dependence, $m(H)$, such as shown in Fig. 2(b) in the main text. The zero-field slope corresponds to the initial susceptibility of the magnetic nanoparticle system and determines the heating rate as suggested by the Rosensweig linear response theory.[5]

To circumvent the practical problem of determining the magnetic mass (or magnetic volume) of nanoparticles at the surface of swimmers by a direct experimental quantification, we determined the slope of the $m(H)$ curves directly by fitting a Langevin function to our data. The argument justifying this is as follows.

Assume the $m(H)$ dependence of a particle can be described by a Langevin function $\mathcal{L}(x)$:

$$m(H) = m_s \mathcal{L}(AH) \tag{S1}$$

where m_s is the saturating magnetic moment, and A is often expressed in theory as $A = \mu_0 m_s / k_B T$ but we keep it as a fit parameter. The magnetic moment can be expressed as $m = MV_m$, where M is the magnetisation and V_m the magnetic volume (i.e. volume of magnetic particles on the swimmers' surface, with all non-magnetic content excluded). Similarly the saturating moment is $m_s = M_s V_m$, where M_s is the saturation magnetisation.

Dividing both sides of Eq. (S1) by V_m gives an equivalent expression in terms of the magnetisation:

$$M(H) = M_s \mathcal{L}(AH) \tag{S2}$$

For small fields $H \to 0$ the Langevin function can be expanded in Taylor series and the above expression rewritten as:

$$M(H) = M_s \frac{AH}{3} \tag{S3}$$

and the slope is:

$$\frac{dM}{dH} = M_s \frac{A}{3} \tag{S4}$$

This slope is equal to the initial susceptibility of magnetic nanoparticles, which according to the Rosensweig linear response theory[5] acts as a proportionality constant determining the generated heat power.

Our swimmers, say S1 and S2, have different amounts of particles on their surfaces, yielding different magnetic volumes V_{m1} and V_{m2}. Given that in both cases the magnetic material is the same (Manganese Ferrite), their M_s must be the same. However, since $V_{m1} \neq V_{m2}$, the magnetic moments $m_{s1} = M_s V_{m1} \neq m_{s2} = M_s V_{m2}$. These differences are reflected in Fig. 2(b) by the $m(H)$ curves having different saturating moments at large magnetic fields, with the highest (smallest) moment observed for swimmers S3 (S1).

Following Eq. (S1), we can express the $m(H)$ curves for the two swimmer types in terms of the Langevin function as:

$$m_1(H) = m_{s1}\mathcal{L}(A_1 H) \qquad \text{and} \qquad m_2(H) = m_{s2}\mathcal{L}(A_2 H) \tag{S5}$$

Fig. 2(b) in the main text shows that fitting these functions to our measurement data gave very good fits.

We can divide both fitted equations by V_{m1} and V_{m2} to reproduce Eq. (2):

$$M_1(H) = M_s\mathcal{L}(A_1 H) \qquad \text{and} \qquad M_2(H) = M_s\mathcal{L}(A_2 H) \tag{S6}$$

Since the magnetic volumes enter equivalently on both sides of Eqs. (S5) and they effectively cancel out to yield Eq. (S6). The magnetic volume is still included within the parameters A_1 and A_2 which are, however, determined by fitting.

Thus any prior knowledge of the magnetic content available on the surface of the individual swimmers is not essential for determining the slopes, which according to Eq. (S4) are:

$$\frac{dM_1}{dH} = M_s\frac{A_1}{3} \qquad \text{and} \qquad \frac{dM_2}{dH} = M_s\frac{A_2}{3} \tag{S7}$$

The values of the fit constants A_k for $k = 1, 2, 3$ obtained by fitting Eq. (S5) to our measurement data are shown in the inset in the main Fig. 2(b). We found A_1 to have the highest value, suggesting the best heating effect is to be associated with S1 swimmers, which is consistent with the magneto-caloric measurements shown in Fig. 2S.

REFERENCES

(1) Matsushita, O.; Jung, C. M.; Minami, J.; Katayama, S.; Nishi, N.; Okabe, A. A Study of the Collagen-Binding Domain of a 116-KDa Clostridium Histolyticum Collagenase. *J. Biol. Chem.* **1998**, *273*, 3643–3648.

(2) Wilson, J. J.; Matsushita, O.; Okabe, A.; Sakon, J. A bacterial collagen-binding domain with novel calcium-binding motif controls domain orientation. *EMBO J.* **2003**, *22*, 1743–1752.

(3) Dunderdale, G.; Ebbens, S.; Fairclough, P.; Howse, J. Importance of Particle Tracking and Calculating the Mean-Squared Displacement in Distinguishing Nanopropulsion from Other Processes. *Langmuir* **2012**, *28*, 10997–11006.

(4) Patino, T.; Arqué, X.; Mestre, R.; Palacios, L.; Sánchez, S. Fundamental Aspects of Enzyme-Powered Micro- and Nanoswimmers. *Acc. Chem. Res.* **2018**, *51*, 2662-2671.

(5) Rosensweig, R. E. Heating magnetic fluid with alternating magnetic field. *J. Magn. Magn. Mater.* **2002,** *252,* 370–374.